Effects of shot peening velocity and coverage on peen forming

Kewen Chen
Jizhan Wu
Qinjie Lin
Jiazan Zhu
Peitang Wei
Huaiju Liu (huaijuliu@cqu.edu.cn)
Chongqing University

Research Article

Keywords: Peening forming, Forming curvature radius, Residual stress, Surface roughness, Equivalent plastic strain

Posted Date: May 26th, 2022

DOI: https://doi.org/10.21203/rs.3.rs-1656095/v1

Effects of shot peening velocity and coverage on peen forming

Kewen Chen[a], Jizhan Wu[a], Qinjie Lin[a], Jiazan Zhu[b], Peitang Wei[a], Huaiju Liu[a*]

a. State Key Laboratory of Mechanical Transmissions, Chongqing University, Chongqing 400030, China

b. China Gas Turbine Establishment, Chengdu 610500, China

*Corresponding author: huaijuliu@cqu.edu.cn

Abstract

As an effective forming technique, peen forming is widely used in sheet metal components with large dimensions. However, the production efficiency is seriously limited as several peening tests are required before actual production. To address this issue, a numerical simulation method of peen forming was proposed. In this work, an elastoplastic peening finite element model was developed to study the relations between process parameters and forming effects. A set of peen forming tests with different coverages and velocities were conducted to validate the model. Results indicate that the maximum errors of converted arc height and forming curvature are less than 5% and 14%, respectively. Additionally, the saturation phenomenon can be observed as the peening coverage reaches 60%. The corresponding depth of the maximum compressive residual stress varies almost linearly with shot velocity.

Keywords: Peening forming; Forming curvature radius; Residual stress; Surface roughness; Equivalent plastic strain

1. Introduction

The integral panel is an essential structural component to connect the skin, flange, and long truss, and widely used as the primary load-carrying structure of modern planes. The integral panel with complex shape directly contributes to the aircraft aerodynamic layout [1], which brings significant challenge to the manufacturing process. On the other hand, the strict requirement for forming performance of wall panel structures brings considerable challenge to the traditional processes [2], such as roll bending, pull forming, and brake pressure. the design and manufacturing of integral panels is an urgent demand in current airplane industry [3] .

Structural components, including integral panels, require to be lightweight while keep high mechanical properties [4]. Besides, integrated panels sometimes require special shapes of complex curvature [5]. This brings great difficulties in the manufacturing process. The peen forming is a practical solution for these challenges. Peen forming has the advantage of flexible operation, controllable cost and does not require mold or die process. Thus, it is suitable for manufacturing large dimension panels. However, the mechanism of peen forming still requires to be discovered. Many machining factors before the process contribute to unexpected plastic deformation. Till now, the selection of process parameters largely relies on engineering experience and test data.

There is indirect experimental method based on standard specimen samples for peen forming studies. The shot peening intensity, Almen Intensity [6], is defined by the arc height of the special specification metal sheets after peening, which is an international common on measurement of shot peening intensity [7]. Though the Almen Intensity test has been applied worldwide for decades, there is still room for improvement in strength definition[8]. The same arc height can be obtained by combining different process parameters, leading to the lack of a unified standard for selecting parameters. Inspired by the Almen Intensity test, Wang et al. [9] directly simulated the effect of a large number of shots on the standard specimen. They made the precise control of peen forming deformation possible, revealing the equivalent relationship between shot velocity and peening intensity in the shot peening forming process. And to optimize stress peen forming process, Miao et al. [10] determined the quantitative relation between peening time, surface roughness and coverage by designing experiments on Almen-sized Al2024 strips. Yang et al. [11] obtained the forming limit of specimens with different thicknesses by establishing the shot peening model of Ti-6Al-4V specimens and successfully acquired the phenomenon of concave deformation caused by high shot peening intensity in the numerical model. Takahiro et al. [12] analyzed the changes of plastic strain distribution with coverage in the peen forming of high-strength Aluminum alloy plate and supposed that increasing the coverage could enhance the deformation effect by expanding the plastic strain to a larger surface area. According to the finite element model calculation, they also found that saturation occurs gradually when the coverage reaches approximately 65% for A7075-T6 plate samples.

The quality evaluation of shot peening should also consider surface integrity factors. However, most indirect experimental studies focus on the final forming result, i.e., the radius of curvature and arch height after peening, while surface integrity parameters are seldom considered. Aiming to explore relationships between process parameters and forming results, FEM numerical model of SAE 1070 spring steel specimens was constructed to explore the effects of peening coverage and shot velocity. The actual peening test was conducted.

2. Experimental procedures

2.1 Material selection and peening treatment

The standard SAE 1070 specimen was taken as the target to be treated, with dimension of $76.1 \times 18.95 \times 1.295\ \mathrm{mm}^3$. The material composition of SAE 1070 is illustrated in Tab. 1.

Tab. 1 SAE 1070 steel element content (wt/%) [13]

C	Mn	Si	S	P	Ni	Cr	Cu
0.68-0.75	0.50-0.80	0.17-0.37	≤0.035	≤0.035	≤0.25	≤0.25	≤0.25

The SP1500 manual pressurized shot peening machine, shown in Fig. 1, was applied. The chamber dimension is $1500 \times 1500 \times 1000\ \mathrm{mm}^3$. The range of mass flow and shot peening

pressure are 0 ~ 30 kg/min and 0 ~ 0.8 MPa, respectively.

During the peening process, the specimen was clamped on the piece holder by screws and nuts. The relative position of the nozzle and specimen was adjusted to make the nozzle align with the center of the specimen. A distance of 150 mm was also kept so that the shots approximately cover the surface of test piece. The S930 hard cast steel shots with 3 mm diameter were selected.

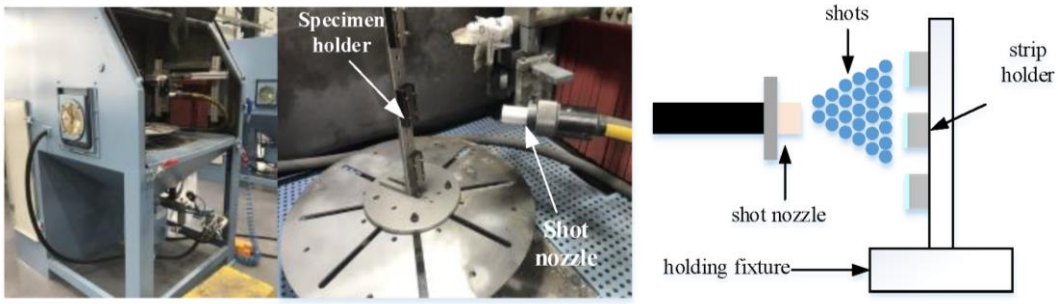

a) Peening equipment b) Peening chamber c) Peening process

Fig 1. Shot peening machine.

2.2 Test method

The test was divided into two aspects, the shaping performance and the surface performance. The shaping performance includes the convex arch height and the curvature radius. The arch height can be measured by an arch height tester, as shown in Fig. 2 (a). The radius of curvature can be calculated by the geometry relation with the assumption of spherical deformation. As shown in Fig. 2 (b), there is a rectangular testing area of $31.75\ \text{mm} \times 15.87\ \text{mm}$ on the tester, and the eventual arch height of specimen is the height difference between center and the midpoint of black lined edges. The geometrical relation between arch height and radius of curvature is displayed in Fig. 2 (c), expressed as:

$$R = \frac{L^2}{8A_h} \tag{1}$$

where L is the chordal or tangential length, A_h and R are the value of arch height and radius of curvature, respectively. The unit for the three parameters is millimeter.

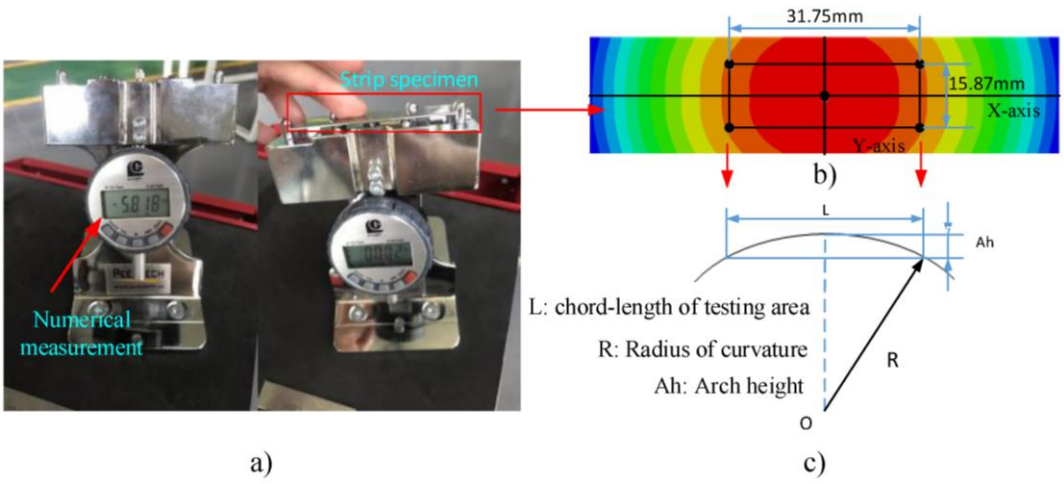

Fig 2. Measurement with the arch height tester

The surface performance is evaluated by residual stress, surface topography and surface roughness. The residual stress of the specimen was measured by a μ-360s portable X-ray diffractometer. Adjust the instrument to be 35 ° to the horizontal plane, and control the working voltage and the current as 30 kV and less than 5 mA, respectively. The surface residual stress of specimen was measured.

The surface topography was scanned by a white light interferometer. Each measuring area is 40×40 μm. Testing parameters are summarized in Tab. 2.

Tab. 2. Measurement objects and testing equipment

Measurement Objects	**Testing Equipment**
Surface topography	Kynex 3D Ultra Depth of field system
Surface roughness	RTEC white light interferometer
Residual stress	μ-360s portable X-ray diffractometer
Arch height and curvature radius	PAO100 Arch height tester

3. Numerical Methodology

3.1 Basic assumptions

Fig. 3 shows the mechanism of peen forming process. As illustrated in the figure, the basic principle of peen forming is similar to shot peening. When shots with a high velocity impact the metal sheet surface, the uneven plastic deformed area will be produced, and stress that brings the sheet a trend of extension will also be induced. To achieve the static equilibrium of stress within the sheet, bending deformation that is required will be generated on the sheet [14].

When the restriction of the metal sheet is canceled, the induced stress returns to the unbalanced state so that the plastic strain layer on the surface extends to all directions horizontally. The increased area of the peened surface makes the metal sheet convex against the shot peening direction to achieve the required curvature shape structure [15]. This process is

illustrated as the bending deformation in the upward bulge direction in Fig. 3 (b) and is named as the spring back process.

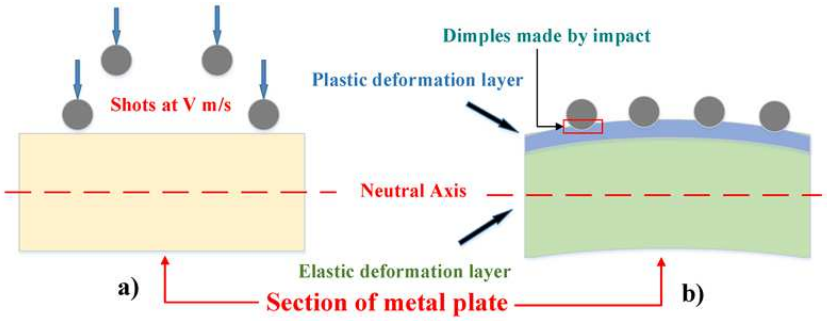

Fig 3. Schematic of peen forming mechanism a) before deformation; b) after deformation

Because the plastically deformed layer is quite thin compared with the entire metal sheet, while the bending deformation under the plastic deformed layer can be supposed as elastic bending, the entire sheet can then be divided into two layers, the upper and lower layers with plastic and elastic deformation, respectively. For the lower elastic layer, the bending moment driven by the residual compressive stress in the upper plastic layer acts as the external moment [16]. As a consequence, to develop the analytical model during the bending deformation process, basic assumptions must be made as follow:

(1) Residual stress leading deformation assumption: the sheet deformation during the spring back process is mainly influenced by the value and distribution of residual stress;

(2) Sheet hierarchical assumption: the sheet can be separated into plastic and elastic layers, and the bending effect from the residual stress in the plastic layer to the lower layer can be seen as external moment;

(3) Uniform peening assumption: the impacting coverage is uniform for the sheet, and since the plastic strain layer is thin, the residual stress is also assumed to be uniformed that there is no concentration of stress;

(4) Sheet free deforming assumption: during the spring back process the sheet is in the free state, not affected by the external force restriction;

(5) The other acceptable assumptions from mechanic in materials, including the normal basic assumption involving bending deformation, such as the plane assumption of bending, the assumption that the sheet material satisfies isotropic and uniformity properties and so on.

3.2 Analysis of bending deformation process

Based on the basic assumptions, parameters involved in the deforming process are illustrated in Fig. 4. The blue part represents the plastic deformed layer while the lower gray part represents the elastic deformed layer. According to Assumptions (2) and (3), if the horizontal plane (X axis) in the Fig. is selected as the center, the moment produced by residual stress M_r reads:

$$M_r = F \times d = (\sigma_c \times S_c) \times \frac{h-\frac{\delta}{2}}{2} = \frac{\sigma_c \delta b (h-\frac{\delta}{2})}{2} \quad (2)$$

Where σ_c is the residual stress of the plastically deformed layer in MPa, δ is the depth influenced by the compressive residual stress of the plastically deformed layer, with unit of mm; S_c is the sectional area of the plastic layer in mm^2, while h and b are the sheet thickness and unit width of the peened area, respectively, both with unit of mm.

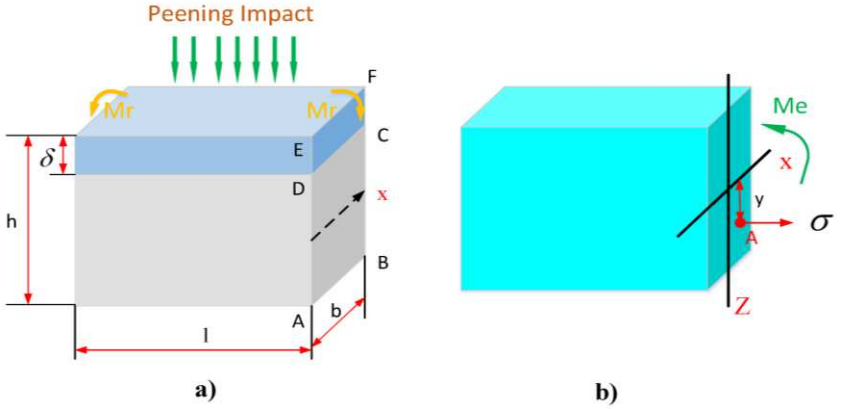

Fig 4. Schematic of a) the peened sheet; b) stress moment with the section

As illustrated in Fig. 4(b), it is obvious that the external bending moment from plastic layer offset with the equivalent moment generated by the internal stress of elastic layer. Then the equivalent moment can be obtained from the internal stress integral of the ABCD section, from the section bending moment formula:

$$M = \int_A \sigma \times y dA \tag{3}$$

In which y is the height difference from a horizontal plane in the integral section to the central axis in the vertical direction, then from the above, it has:

$$M_e = \int_{Ae} \sigma(z) \times y dA = \int_0^{h-\delta} \sigma(z) \times \left(\frac{\mathrm{h}-\delta}{2} - \mathrm{z}\right) \times b dz$$
$$= \int_0^{h-\delta} \frac{E \times \varepsilon(z)}{1-v} \times \left(\frac{\mathrm{h}-\delta}{2} - \mathrm{z}\right) \times b dz \tag{4}$$

Where M_e is the external equivalent moment generated by the internal stress of the elastic layer (MPa), $\sigma(z)$ is the stress at height of z, and combined with the strain expression of bending deformation, $\varepsilon = \frac{y}{R}$, the expression (4) becomes:

$$M_e = \int_0^{h-\delta} \frac{E}{1-v} \times \frac{y^2}{R_e} b dz = \frac{1}{R_e} \frac{E}{1-v} \int_A y^2 \, dA = \frac{E}{1-v} \frac{I_e}{R_e} \tag{5}$$

Where R_e is the radius of curvature after bending, I_e is the moment of inertia of section ABCD; since the plane assumption of bending, this section is rectangular, thus

$$I_e = \frac{bH^3}{12} = \frac{b(h-\delta)^3}{12} \tag{6}$$

Then substituting it into Equation (5), the basic function of radius of curvature can be converted as:

$$R_e = \frac{EI_e}{M_e(1-v)} = \frac{Eb(h-\delta)^3}{12M_e(1-v)} \tag{7}$$

Now from Assumption (4), the internal static equilibrium should be satisfied, that the external moment and the equivalent moment from the internal stress of material can be offset as $M_r = M_e$, then the M_e in expression (10) can be replaced by M_r of expression (2):

$$R_e = \frac{Eb(h-\delta)^3}{12(1-v)} \frac{2}{\sigma_c \delta b(h-\frac{\delta}{2})} = \frac{E(h-\delta)^3}{6(1-v)\sigma_c \delta(h-\frac{\delta}{2})} \tag{8}$$

Which is the relationship between the generated radius of curvature and sheet material

properties (E, v), the residual stress distribution (σ_c、δ) and the geometry dimension of the sheet.

In the above expression of radius of curvature, the affecting result from impacting stage is defined in the residual stress value and depth. While from the generalized strain energy function,

$$W = \frac{1}{2}F \times \Delta \tag{9}$$

Where F and Δ are the generalized force and displacement respectively, then the strain energy W_p of the deformed body relative to the neutral plane can be represented as:

$$W_p = \frac{F\Delta}{2} = \frac{(\sigma S)\times(L\varepsilon)}{2} = \frac{1}{2}\overline{\sigma_c}b\frac{(h+\delta)}{2} \times 2 \times L\overline{\varepsilon_c} = \overline{\sigma_c}\overline{\varepsilon_c}Lb(h+\delta)/2 \tag{10}$$

In which $\overline{\sigma_c}$ is used to describe the averaging value of equivalent stress in the whole metal sheet, and $\overline{\varepsilon_c}$ is the averaging equivalent strain; considering the plane stress state assumption, it reads:

$$\overline{\sigma_c} = \sigma_x = \sigma_y = \sigma_c \tag{11}$$

Then from the radius function of bending deformation, $\varepsilon = \frac{y}{R}$ in which y is the distance from curved surface, so that:

$$\overline{\varepsilon_c} = 2\varepsilon_x = 2\varepsilon_y = 2 \times \frac{h-\frac{\delta}{2}}{2R} = \frac{h-\frac{\delta}{2}}{R} \tag{12}$$

Relative to the entire system, the equilibrium function of energy is:

$$W = W_p + W_e + W_f = \lambda W \tag{13}$$

Where W is the energy from shot impacts, W_p and W_e is the energy of plastic and elastic strain respectively, while W_f is the friction loss during impacting and λ is energy converting coefficient. Equations (12) and (13) can be substituted into Eq. (11) as:

$$\sigma_c = \frac{2\lambda WR}{lb(h+\delta)(h-\frac{\delta}{2})} \tag{14}$$

Taking Equation (14) into (8), the relation between impacting energy and formed radius of curvature is obtained:

$$R_e = \sqrt{\frac{Elb(h-\delta)^3(h+\delta)}{12\lambda W\delta(1-v)}} \tag{15}$$

To make the function much closer with normal process parameter, the total flying kinematic energy of shot before the impact can be expressed from Kinetic energy formula:

$$W = \frac{mV^2}{2} = \frac{V^2}{2} \times \rho \times \frac{4\pi r^3}{3} = \frac{2\rho V^2\pi r^3}{3} \tag{16}$$

Equation (15) can be converted with (16) as:

$$R_e = \sqrt{\frac{Elb(h-\delta)^3(h+\delta)}{8\lambda\rho V^2\pi r^3\delta(1-v)}} \tag{17}$$

However, in the field of engineering practice, if the thickness of uniform residual stress layer is negligible compared with the entire h, then the above can be simplified into:

$$R_e = \sqrt{\frac{Elbh^4}{8\lambda\rho V^2\pi r^3\delta(1-v)}} \tag{18}$$

The derived theoretic model will be implemented in the following plastic FEM simulation.

3.3 Finite element model

3.3.1 Simulation flow of peen forming

From the derivation in the last section, the peen forming process can be divided into two stages, the collision impact stage (explicit calculation) and spring back stage (implicit calculation). ABAQUS Standard/Explicit modules are combined to make the simulating calculation, that the whole coupling calculation process is given in Fig. 5.

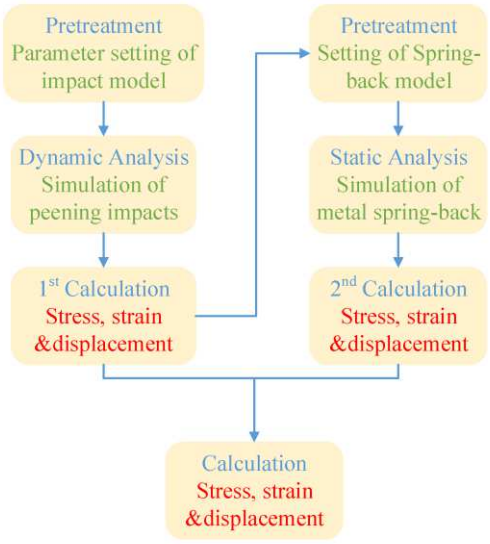

Fig 5. Schematic diagram of explicit and implicit calculation process of ABAQUS model

The generation of random shot impact positions is implemented in an in-house code and adopted in a pre-process, by compiling the re-developmental Python program for ABAQUS. As a first step, a certain number of shots are randomly generated in the area above the target, and then the created contact relationship is given between the target and each shot. The number of shots for a certain coverage is calculated by the impacting area and dimple dimension through the Avrami formula [17]. The related calculation can also be quite efficient if is compiled in to functions, and the formula is show below:

$$C = 1 - e^{-A_r} = 1 - e^{-N\frac{\pi d^2}{4A_p}} \tag{19}$$

where C is the coverage to be reached for the surface, and N is the required number of shots, while A_r is the indentation ratio that is the ratio of the total area of the dimples to the total peened area on the sheet surface, in which d is the diameter of the dimple (mm) and A_p is the area of the peened region (mm^2). The dimple dimension is obtained from the single shot impacting model.

3.3.2 Parameters of finite element model for shot peening

In this paper SAE 1070 steel is selected as material to be peened, whose dimension is $76.1\ (\text{length}) \times 18.95\ (\text{width}) \times 1.295\ (\text{thickness})$ in mm. In terms of material properties, since shot impact is a shock load, severe plastic deformation will occur to the plate in a very short time, it is important to select an appropriate hardening model. Therefore, the Johnson-Cook model that can describe the influence of high pressure and high strain rate on the yield stress of materials are selected [18]. The constitutive model is represented as:

$$\sigma = (A + B\varepsilon^n) \times \left[1 + Cln\left(\frac{\varepsilon}{\dot{\varepsilon}_0}\right)\right] \times \left[1 - \left(\frac{T-T_0}{T_m-T}\right)^m\right] \quad (20)$$

where σ is the obtained equivalent stress, $\dot{\varepsilon}_0$ and T_0 are the quasi-static strain rate and temperature reference, while ε and T are the considered strain rate and temperature respectively, and T_m is the melting point of metal.

Constants A, B, C and n respectively represent five material parameters obtained from the test, and the material properties selected by literature[19] are given in the table below.

Tab. 3. SAE 1070 steel Johnson cook model parameters [19]

A（MPa）	B(MPa)	C	n	M(℃)
1048	600.8	0.0134	0.234	0

The S930 hard cast steel shot with 3 mm diameter is selected as the shot, and its material property is set to the conventional isotropic model.

The symmetric model is considered to reduce the calculation cost, so that the 1/4 specimen model was built up. The symmetric constraints in both length and width direction were imposed to the outer surface to simulate the entire process specimen being peened.

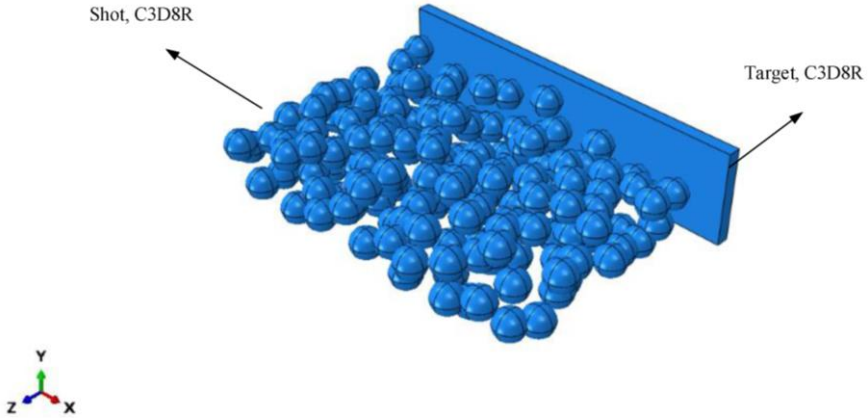

Fig 6. The impacting model of the peening process

For peening coverage, an increment of 10% is set to explore the influence of the parameter between 20% and 80% sequentially on shaping result and surface performance. While for shot velocity, 40% is set as the coverage and 5 m / s is the interval. Then with the empirical formula (21) [16] and comprehensive consideration on the working capacity of the equipment used, the selected range of exploration is between 20 m/s and 60 m/s.

$$V = \frac{163.5P}{1.53M+10P} + \frac{295P}{0.598+10P} + 483.P \quad (21)$$

where P and M are the air pressure and flow rate working parameters, and V is the calculated impacting velocity of the discharged shots. In addition, the impacting coverage of each specimen is controlled by the peening time during the test.

4. Results and Discussion

4.1 Effect of shot peening coverage on forming

4.1.1 Effect of shot peening coverage on shaping result

The comparison of arch height between the specimen measured in the test and the numerical simulation is given in Fig. 7 below. From the fitting curve of the numerical model, when the coverage rises from 20% to 50%, the increases of arc height by nearly 0.145 mm. When the coverage rises by the next 30%, the growth of arc height is limited to only 0.040 mm. It is clear that saturation convergence occurs during the process. Further, when the number of shot impacts increases by 2 times but the maximum arc height increases by less than 10%, it can be supposed to be reaching saturation [10,21]. This is based on the definition of the saturation point of the peened specimen and the summarized expression is below:

$$A_h(2N_s) = 1.1A_h(N_s) \tag{22}$$

where A_h is the arch height produced by a certain number of shot impacts, and N_s is the number of impacts to reach the saturation point. After comparison, it can be discovered that when central coverage is 60%, it can be approximately regarded as the saturation point of the shot impact mode.

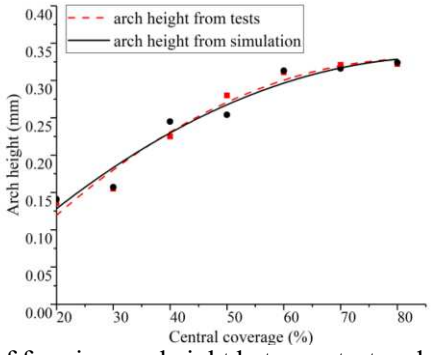

Fig 7. Comparison of forming arc height between test and numerical simulation

The curvature radius of each arch height value is also calculated by formula (1), shown in Fig 8. The saturation of coverage is clearly indicated as the radius value stays nearly stably at 400 mm when coverage grows beyond 60%. Besides, the two fitting curve reveals that they coincide with each other well, with a maximum error rate of only 5.2%. In other words, the peen forming experiment evaluates the plastic FEM model well.

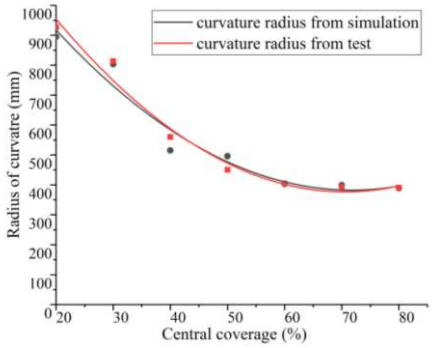

Fig 8. Comparison of forming radius of curvature between test and numerical simulation

4.1.2 Effect of shot peening coverage on surface performance

The influence of the coverage parameter is described by three measurements the residual stress, equivalent plastic strain and surface morphology. In the first place, Fig 9 (a) summarized the calculated residual stress distribution before the spring back process. It can be observed that the absolute value of residual stress in the specimen increases significantly with the rise of peening coverage, from roughly 500 MPa to 1400 MPa. Besides, there is a phenomenon that though the residual stress value increases with the coverage gradually, the distributed depth stays at nearly the same level. The residual stress distribution after spring back process is also presented in Fig 9 (b). When the spring back deformation occurs, the compressive residual stress in the specimen surface decreases significantly. When coverages arrive at around 60%, the tensile stress appears. The reason for the phenomenon can be considered that when the central area drives the surrounding regions to bulge upward, the bending deformation causes the tension of surface metal fibers. The fiber tension then results in the decrease of surface residual compressive stress [22]. Detailly, the maximum tensile surface stress is around 200 MPa near the saturation point of 60% central coverage, and then decreases to close to 0 again. It can also be suggested that when the coverage reaches saturation point, the degree of bending deformation hardly changes, but more impact times introduce greater average residual compressive stress and more uniform distribution. Eventually, the value of surface residual stress decreases again after the rebound.

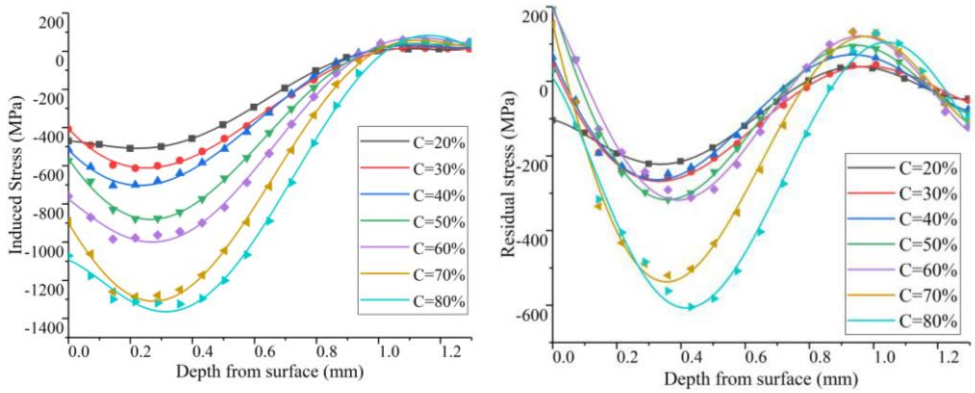

a) Induced stress profile after shot peening b) Residual stress profile after springback

Fig 9. Comparison of stress profile with removing boundary restriction under different coverage

The distribution of Equivalent Plastic Strain (*PEEQ*) of the peened target [23] is also extracted in the same direction. *PEEQ* is a physical quantity used to determine the position of the yield surface of the strengthened material, which is a common measure of plastic strain in ABAQUS. The definition of *PEEQ* is similar to equivalent stress and strain, and the calculation is completed according to the fourth strength theoretical formula of equivalent stress. The computing of PEEQ in ABAQUS is:

$$PEEQ = \bar{\varepsilon}^{p}\mathrm{l}_0 + \int_0^t dpdt \tag{23}$$

in which $\bar{\varepsilon}^{p}\mathrm{l}_0$ is the initial *PEEQ* of the material and dp is the increment of it.

Fig.10 is the extracted result of PEEQ. The maximum PEEQ in each coverage model before spring back appears at a depth of around 0.14 mm below the surface, and then the PEEQ approaches 0 when the depth is close to 1.0 mm. After the spring back process, the peek value of PEEQ is almost eliminated and becomes 0. And this is why it is not presented in Fig.10. The spring back deformation process is considered to promote the uneven plastic deformation in the released specimen, then it gradually tends to be uniform under the action of bending. Comparing the distribution of PEEQ and residual stress, it can be observed that when the PEEQ value gradually approaches 0, it just approximates the turning point of residual stress from

compressive to tensile. In other words, it is consistent with the theory produced by non-uniform plastic deformation.

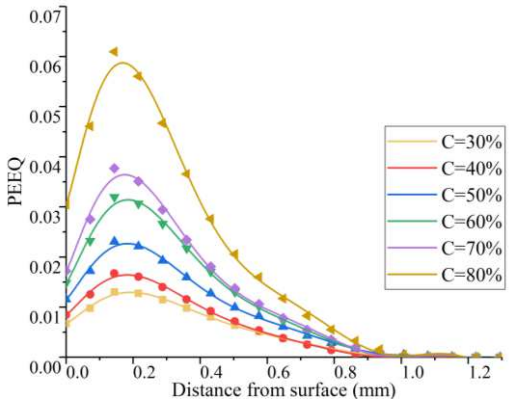

Fig 10. Comparison of PEEQ resulted from impacts under each coverage

In addition, by extracting the displacement of nodes on the specimen surface, the surface morphology is obtained. Among the many parameters to quantify surface roughness based on tactile profile, the *Sa*, the arithmetic mean of surface roughness parameter is the most intensive and commonly used parameter to characterize the level of surface roughness so far [24]. For the arithmetic mean value of three-dimensional surface roughness, the calculation expression is as follow:

$$Sa = \frac{1}{n}\sum_{i=1}^{n}|Z_i| \tag{24}$$

where Z_i is the coordinate in the peening direction, n is the number of nodes. Besides, another 3D surface roughness parameter *Sq*, referring to the 3D root mean square value is also taken advantage to represent the morphology. *Sq* is a significant parameter in the surface state as it will affect the abrasiveness, sealing and wettability of the material surface, The calculating expression of *Sq* is defined as (25):

$$Sq = \sqrt{\frac{1}{n}\sum_{i=1}^{n}Z_i^2} \tag{25}$$

The calculated surface roughness *Sa* and *Sq* parameters from surface morphology are summarized in Fig. 11. While the *Sa* roughness increases almost linearly, the *Sq* with quadratic root character converges after the coverage reaches 50%. Therefore, considering the calculation formulas of the two roughness, it can be considered that the roughness changes linearly with the central coverage.

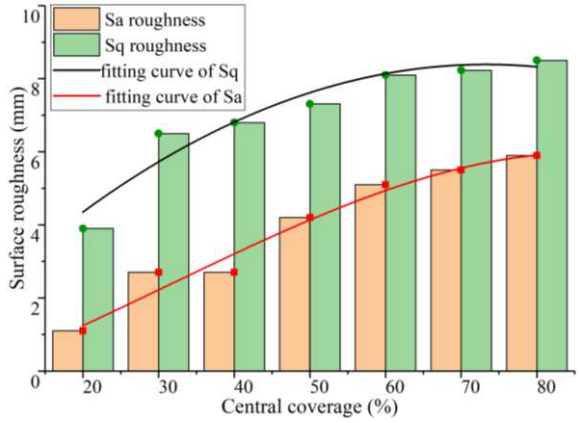

Fig 11. Variation of two roughness parameters with central coverage

4.1.3 Results of shot peening coverage test

The surface residual stress value of the specimen in the coverage parameter model verification experiment is summarized in Fig.12. It should be declared that the value is obtained by measuring each specimen at five positions in its length direction, and then calculating their average. The black solid line represents the fitting curve of the measured surface roughness value. For actual test pieces, it will introduce initial residual stress to the specimen from the manufacturing process, which is not considered during the Plastic FEM simulation model. On this basis, the non-peened test specimen should be taken as the benchmark. The red dotted line is used to represent the interpolation fitting curve of the surface residual stress value. With the two solid lines, the relative change value of the surface stress after peen forming is described. It can also be observed that with the growing coverage, the measured surface residual stress increases gradually until reaching the peak at the coverage of 60%. And then it starts to decrease, for which the general trend is in keeping with the variation in the simulation. Thus, from the perspective of various tendencies, the test results can qualitatively verify the conclusions in the Plastic FEM simulation.

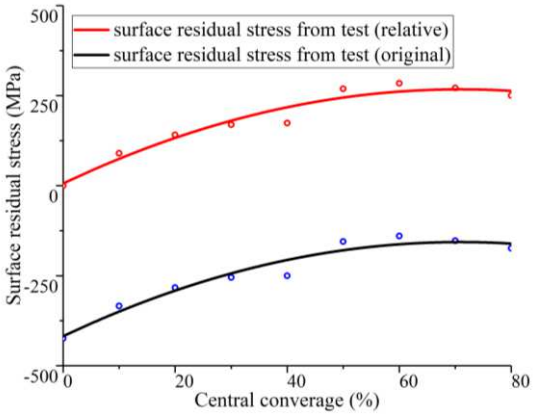

Fig 12. Fitting curve of surface residual stress measured by experiment with coverage

For the surface morphology, the scanning data processing and visualization is completed with the help of Gwyddion software, and the morphology of each measurement point at an area of 40×40 μm is output. In addition, during the calculation of surface roughness value, the highest-order polynomial function in Gwyddion software is used to eliminate the influence of distinct curvature radius as much as possible. In such case the specimen surface is analyzed as a plane. However, the disadvantage of this method is that while it reduces the influence of the bulge height of the test specimen, it will also reduce the dimple fluctuation in the calculation. Then the calculated roughness value will be too small. Nevertheless, though the numerical value cannot be directly quantified according to the simulation results, it can be verified qualitatively through the changing trend of roughness value with coverage parameters. The measured surface morphology and roughness parameters in the experiment are summarized in Fig. 13.

It can be seen that with the increase in coverage rate, due to the violent impact of shots, the processing trace is covered by dimples on larger scale. Besides, the extrusion deformation caused by the overlap between dimple areas is gradually intense, resulting in more undulating peaks and valleys on the specimen surface, which is rougher on the macro level.

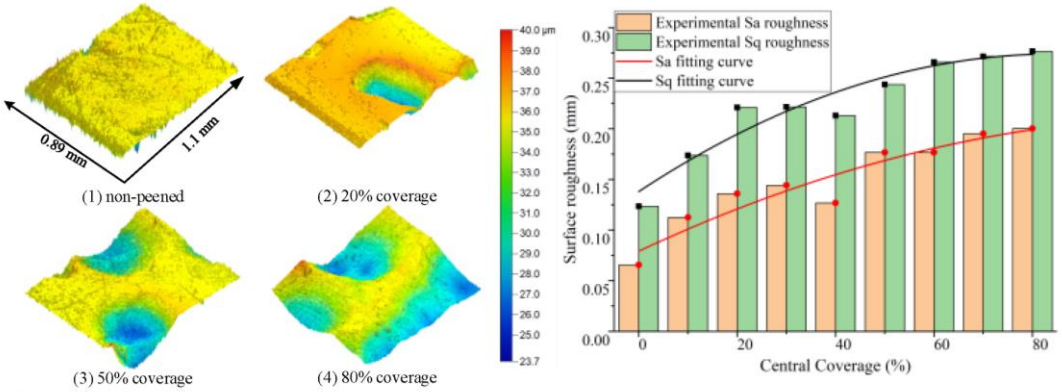

(a) Surface morphology under each peening coverage (b) Variation of roughness with coverage measured in test

Fig 13. Surface morphology and roughness variation of specimen under each peening coverage

According to the fitting curve in Fig. 13(b), it can be seen that when the coverage increases from non-peened to 40%, the calculated roughness *Sa* changes from 0.08 mm to around 0.15mm. When the coverage rises continuously to 80%, *Sa* also increases significantly to around 0.21 mm. There is no obvious slow convergence in its growth, and it can still be considered to have linear variation characteristics. Therefore, it can be supposed that the simulation results are verified qualitatively.

Based on the simulation and experimental analysis of the peening coverage parameter, it can put forward a hypothesis of the phenomenon in the process that roughness increases with coverage. The essence can be considered that the local uneven plastic deformation introduced by shot impacts gradually covers the whole surface of work piece. Then under the cumulative effect, the plastic regions underneath each dimple are combined with each other to gradually form a global equivalent plastic deformation layer. As the coverage in this model does not exceed 100%, the overlap of the coverage area is not serious, and thus, there is a linear correlation with the coverage. For the equivalent plastic deformation region, it can be considered that the discrete impact can no longer have a significant impact on the local surface roughness of the region. Specifically, with the increase of coverage, all surface integrity parameters except roughness increase, and the increased range decreases gradually. The reason is that when the peened target reaches near the saturation point, an equivalent plastic deformation layer has been formed on the surface so that the increment of impacting coverage cannot significantly affect the morphology of the deformation layer.

4.2. Effect of shot velocity on forming

4.2.1 Effect of shot velocity on shaping result

To present and evaluate the precision of the velocity model, the forming experiment of shot velocity is also conducted during the simulating calculation. The comparison between numerical and experimental results is summarized in Fig. 14. In terms of simulation, with the raising of shot velocity, the increase of arc height has stronger linear characteristics without obvious saturation, compared with the condition of coverage parameter. Starting at 20 m/s, the arc height caused by lifting the shot velocity of 10 m/s is 0.090 mm, 0.149 mm, 0.195 mm, 0.226 mm and 0.253 mm respectively, which increases by 65.6%, 116.7%, 151.1% and 181.1% respectively compared with 20 m/s.

In terms of the test result, it can be seen that with the gradual increase of shot velocity from 20 m/s, the arc height of the test specimen increases also approximately linearly without obvious saturation convergence. Compared with the coverage model verification experiment, the deviation between the simulation result and the experimental data in this comparison is large, that error of the arc height fitting curve is approximate 7.25% at the maximum.

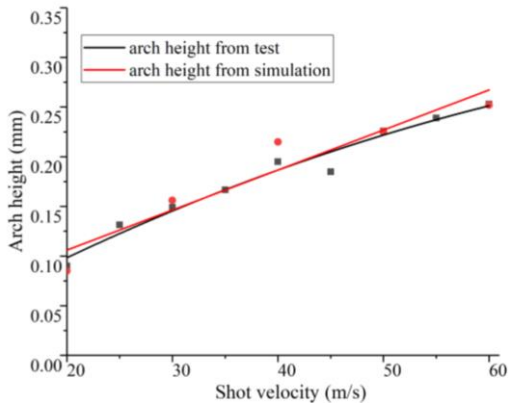

Fig 14. Comparison of variation of forming arc height with shot velocity between experiment and numerical simulation

The radius of curvature is also calculated by formula (1) and summarized in Fig 15. It seems that the fitting error between numerical calculation and test result is much larger, that the maximum is at 13.9%. While for the increase of error, it can be interpreted that the controlling valves for the peening pressure and flow rate equipped in the peening machine are not completely precise, contributing to the bias of actual shot velocity. However, due to the request of less than 15%, it can be considered that the shaping result obtained by the two are consistent, which refers to the fact that this experiment has verified the conclusion of the shot velocity model in forming effect and confirmed the reliability of its data.

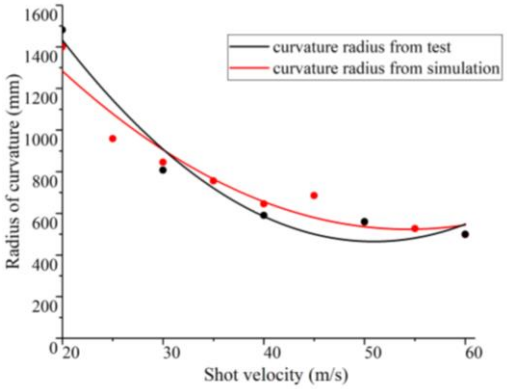

Fig 15. Comparison of variation of forming arc height and radius of curvature with shot velocity

4.2.2 Influence of shot velocity on surface performance

In the aspect of residual stress, the stress distribution of the specimen before and after the spring back process is extracted and compared in Fig.16, and it is obvious that the residual stress growths significantly with the shot velocity. With the increase of shot velocity, the residual compressive stress of the specimen not only increases generally but also extends in a deeper direction. To clarify the variation of distribution, the depth of the maximum average residual compressive stress and the critical depth when the residual stress changes from negative to positive is extracted, and also presented in Fig.17.

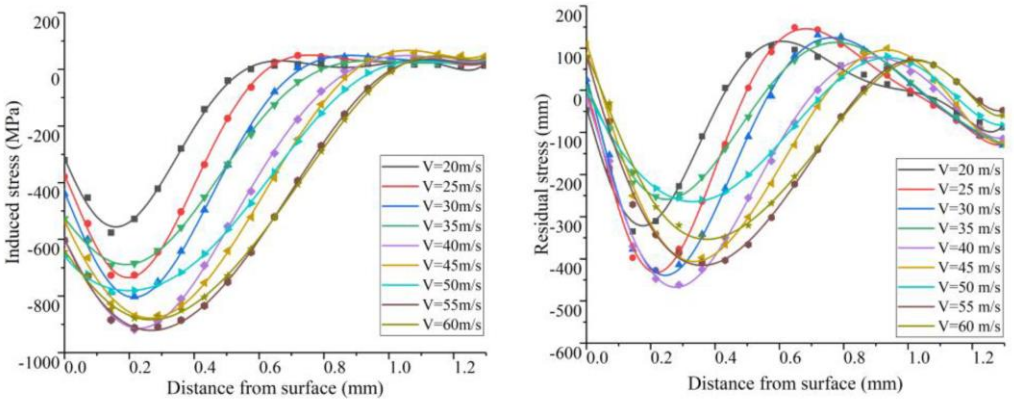

a) Induced stress field before spring back process b) Residual stress field after spring back process

Fig 16. Comparison of residual stress of specimen before and after spring back at each shot velocity

For the two extracted depth variations in Fig.17, the depth at which the residual stress eliminate increases approximately linearly and significantly with the increase of shot velocity, either before or after spring back.

In Fig.17 (a), it can be observed that increasing shot velocity causes a shift of the turning position of compressive stress before bending towards a deeper region linearly, while the depth of the maximum stress does not vary significantly, compared with the condition after the bending. While in Fig. 17(b), the two depths both show linear growth properties. In addition, it can be observed that the process of bulge deformation reduces the depth of 0 point by 0.173 mm on average. The principle can be considered that the tensile deformation caused by bending deformation partially offsets the residual compressive stress value, reduces the overall level of internal stress, and moves up the position of 0 value point.

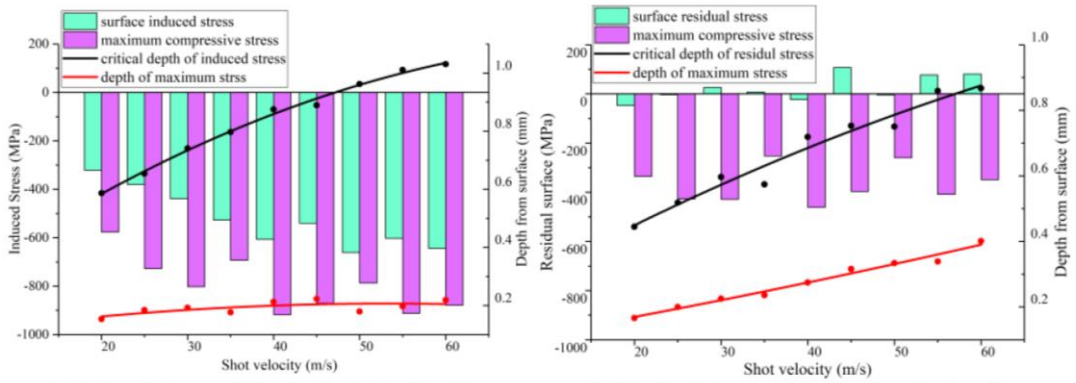

(a) Induced stress and distribution before bending (b) Residual stress and distribution after bending

Fig 17. Comparison of residual stress of specimen before and after spring back at each shot velocity

The extracted PEEQ field is given in Fig. 18(a). It can be clearly observed that with the shot velocity growing from 20 m/s to 60 m/s, the distribution range of PEEQ gradually extends, while the depth containing the maximum PEEQ value roughly stays at the same level. To be more precise, the extracted depth of the maximum PEEQ value and the depth at which the peak value is reduced to 10^{-5} (suppose as the 0 value) depth are sorted in Fig. 18(b). It is clear that the depth containing PEEQ of maximum value almost stays stably at approximate 0.15 mm. Combing with the variation of the depth of the maximum residual compressive stress, the figure for the maximum plastic strain has no obvious correlation with the shot velocity, which is consistent with the relevant data in the literature [25] and literature [26]. Thus, it can be considered that the variations of the two have a corresponding relationship, that the residual compressive stress increases with the increase of PEEQ. And there is also a positive correlation between the distribution depth. With the increase of shot velocity, the depth of PEEQ to 0 increases significantly, but it tends to be saturated after the shot velocity reaches 45 m/s.

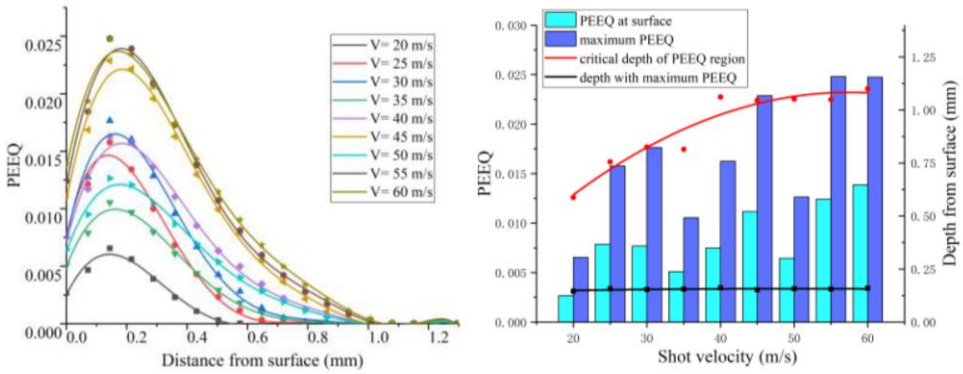

a) PEEQ field with each velocity　　b) variation of PEEQ distributed depth

Fig 18. PEEQ distribution of speciemen after peening with each shot velocity

In terms of surface morphology quantification, the two roughness parameters under each impact velocity, *Sa* and *Sq*, are calculated and combined in Table 4. It can be considered that with the increase of shot velocity, the greater impact force causes greater and deeper depression on the surface of the specimen, making the characteristics of crest and trough of concave convex fluctuation more obvious, and the surface roughness value larger.

Tab. 4. Influence of shot velocity to the two roughness parameters

Shot velocity	*Sa* roughness	*Sq* roughness
20	1.034	2.336
25	1.509	3.176
30	2.005	4.089
35	2.549	4.998
40	2.856	5.583
45	3.303	6.415
50	3.649	7.120
55	3.951	7.610
60	4.252	8.308

From the table, taking 20 m/s, 30 m/s, 40 m/s, 50 m/s and 60 m/s as examples, the corresponding roughness *Sa* values are respectively 1.034 μm, 2.005 μm, 2.856 μm, 3.649 μm and 4.252 μm. With the increase of shot velocity, *Sa* roughness increases by 93.9%, 176.2%, 252.9% and 311.2% respectively compared with 20 m/s. While the corresponding *Sq* roughness parameters are 2.336 μm, 4.089 μm, 5.583 μm, 7.120 μm and 8.308 μm, which increased by 75%, 140.0%, 204.8% and 255.7% compared with the situation of 20 m/s. During shot peening, the impact kinetic energy of shots on the target has a great impact on the roughness of the peened surface. With the increase of its velocity, the surface roughness parameters *Sa* and *Sq* almost increase linearly[10].

4.2.3 Analysis of shot velocity experiment results

In the field of residual stress, the measured surface residual stress is processed and compared with the result from the plastic FEM simulation in Fig. 19. Similarly, compared with the ideal situation where the initial residual stress is not included in the numerical simulation,

the residual stress levels of the actual specimen are illustrated as the black dots in the Fig 19. When the shot velocity varies from 20 m/s to 60 m/s, the stress changes from -346 MPa to -192 MPa. It is significantly lower than the numerical simulation result from -47 MPa to 82 MPa, which are represented by blue points. Besides, to observe the relationship between their varying trends, the dots are connected and fitted by the black and blue lines respectively. Then the relationship between residual stress and shot impact velocity in the experiment and numerical model can be summarized as follow:

$$S_s(v) = S_t(v) + k \times S_t(0) \tag{26}$$

In which $S_s(v)$ is the residual stress on the surface of the formed target when the shot velocity is at v in the numerical simulation under the ideal condition of no initial stress. And $S_t(v)$ is the actual measured surface stress in the experiment, and $S_t(0)$ represents the initial stress as the shot velocity is at 0, k is the conversion coefficient. In Fig. 19, the red line is the revised experimental surface residual stress curve with k = 0.7 according to the above relationship. It fits well with the simulated curve. Therefore, it can be considered that the shot velocity parameter model has been well verified.

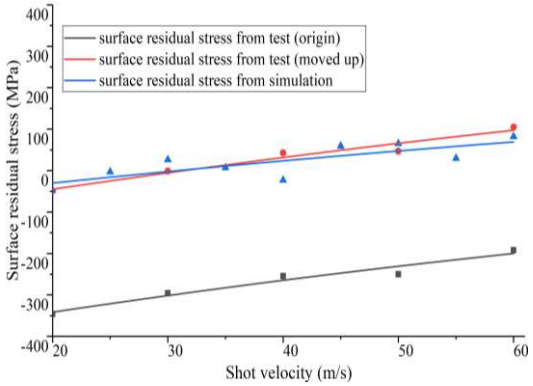

Fig 19. Comparison of variation of surface residual stress with shot velocity between expriment and numerical simulation

By combining the simulating and experimental results of shot velocity parameter exploration, this paper proves that the equivalent plastic deformation layer caused by shot peening impact influences the forming through the scope and vertical two levels. In the level of scope, by increasing the area proportion of surface plastic deformation area, the target surface can obtain a larger equivalent moment to drive bending deformation, so as to improve the shaping result, for which the implementation methods include prolonging shot peening time to obtain higher shot peening coverage. While for the vertically influencing level, by introducing the induced stress into the deeper region so that the region of the target is transformed into an equivalent plastic deformation layer, as to drive the generation of rebound deformation, and eventually obtain a more significant shaping result, which can be realized by improving the impact kinetic energy of the shot.

Conclusions

A numerical method of peen forming is proposed to explore the forming mechanism. Simulation is verified by experimental results. Conclusions can be drawn as follows.

(1) The bending deformation during the peen forming process is analyzed and the relation between forming curvature radius, shot impact energy and material parameters is derived. An elastoplastic FEM model of peen forming is developed. It is discovered that an average difference of 0.173 mm exists between before and after spring back deformation in velocity exploration.

(2) Comparing the calculation result and peening experiment, the hypothesis of equivalent plastic deformation layer is put forward, that it affects the forming effect from the

scope level and vertical level. The scope level is realized by the increase of area ratio of plastic deformation area resulting from high coverage. While the vertical level is introducing greater stress into a deeper region to produce significant deformation driving effect.

(3) The established model and its conclusions are verified and discussed through a shot peening experiment from both the quantitative and qualitative points of view. And the conversion calculation formula between the ideal specimen and the initial stress case is discovered. The conversion coefficient in the condition of this paper is creatively proposed to be 0.7, which further supplements the proposed equivalent plastic deformation layer hypothesis.

Statements & Declarations

Funding

The work is supported by the National Science and Technology Major Project of China (2019-VII-0017-0158).

Conflicts of interest

The authors declared that they have no conflicts of interest to this work. We declare that we do not have any commercial or associative interest that represents a conflict of interest in connection with the work submitted.

Availability of data and material

The authors declare that the data and the materials of this study are available within the article.

Code availability

Not applicable here.

Ethics approval

Ethical approval was obtained from the Chongqing University Ethics Committee.

Consent to participate

Written informed consent was obtained from individual or guardian participants.

Consent for publication

The authors agree to publication in the Journal in Spring.

Authors' contributions

Kewen Chen and Huaiju Liu designed the experiment. Jizhan Wu and Qinjie Lin measured the surface morphology and the residual stress. Peitang Wei, Jizhan Wu and Qinjie Lin fabricated the samples. The data analysis was performed by Kewen Chen and Jizhan Zhu. The paper was written by Xiuhua Zhang. All the authors discussed, reviewed, and commented on the manuscript.

Reference

[1] S. Lu, Y. Zhu, Z. Liu, Y. Guan, S. Cheng. Research progress of high energy ultrasonic peening forming and sizing technology. Aeronautical Manufacturing Technology, 2013, 53(11): 45-47.

[2] Y. Zeng, J. Shang, C. Xu, M. Qiao, J. Wang, J. Dong. Shot peen forming of ARJ21 large integral wing skin panels with supercritical airfoil. Aeronautical Manufacturing Technology, 2007(3): 38-41.

[3] Y. Peng, J. Chen, L. Yang, Y. Wang. Study on elongation after shot peen forming for integral panel of large aircraft. Aeronautical Manufacturing Technology, 2017,57(9): 97–100, 105.

[4] A. Zhao, X. Zhang, G. Gao, L. Liu, Y. Wang. A systematic method of shot peen forming of large integral wing skin panels. Acta Aeronautica et Astronautica Sinica, 2019, 40(2): 522635.

[5] J. Chen, J. Dang. Analysis of key problems during spread modeling on large dual-curvature integral panel with high ribs. Aeronautical Manufacturing Technology, 2015(1)：64-65.

[6] H.Y. Miao, S Larose, C Perron. M. Levesque. An analytical approach to relate shot peening parameters to Almen intensity, Surface & Coatings Technology, 2010, (205): 2055-2066.

[7] F. Tu, D. Delbergue, T. Klotz. A. Bag, H.Y. Miao, C. Bianchetti, M. Brochu, P. Bocher, M. Levesque. Discrete element-periodic cell coupling model and investigations on shot stream expansion, Almen intensities and target materials. International Journal of Mechanical Sciences, 2018, (145): 353-366.

[8] Fuchs H O. Defects and virtues of the Almen intensity scale[C]//Proceedings of the 2nd International Conference of Shot Peening ICSP. 1984, 2: 74-78.

[9] C. Wang, W.G. Li, J. Jiang, X. Chao, W. Zeng, J. Xu, J. Yang An Improved Approach to Direct Simulation of an Actual Almen Shot Peening Intensity Test with a Large Number of Shots. Materials, 2020, (13): 1-23.

[10] H.Y. Miao, D. Demers, S. Larose, C. Perron, M. Levesque, Experimental study of shot peening and stress peen forming. Journal of Materials Process Technology, 2010, (210): 2089–2102.

[11] F. Yang, Y. Gao, Predicting the Peen Forming Effectiveness of Ti-6Al-4V Strips With Different Thicknesses Using Realistic Finite Element Simulations, Journal of Engineering Materials and Technology, 2016, (318): 1-8.

[12] T. Ohta, S. Sato，Numerical Analysis of Peen Forming for High-Strength Aluminum alloy Plates. The Japan Society for Technology of Plasticity, 2021, (61): 115-123.

[13] AMS, SAE Standard. "Aerospace Material Specification SAE J403." Chemical Compositions

of SAE Carbon Steels (2001).6.

[14] H.Y. Miao, S. Larose, C. Perron. M. Levesque, Numerical simulation of the stress peen forming process and experiment validation, Advances in Engineering Software, 2011, (42): 963-975

[15] Y.B. Hu, W. Zhang, W. Jiang, L. Cao, Y. Shen, H. Li, Z. Guan, J. Tao, J. Xu. Effects of exposure time and intensity on the shot peen forming characteristics of Ti/CFRP laminates, Composites: Part A 2016, (91): 96-104

[16] J. Wu, H. Liu, P. Wei P, C. Zhu, Q. Lin, Effect of shot peening coverage on hardness, residual stress and surface morphology of carburized rollers, Surface & Coating Technology 2020, (384): 125273.

[17] A.H. Astaraee, S. Bagherifard, A. Bradanini, P. Duo, S. Henze, B. Talor, M. Guagliano. Application of shot peening to case-hardened steel gears: the effect of gradient material properties and component geometry, Surface and Coatings Technology, 2020, (398): 126084.

[18] T. Zhang, L. Lei, S. Lu, H. Gong. Simulation of prestressed ultrasonic peen forming on bending deformation and residual stress distribution. The International Journal of Advanced Manufacturing Technology, 2018, (98): 385-393.

[19] M. Jebahi, A. Gakwaya, J. Levesque, O. Mechri, K. Ba. Robust methodology to simulate real shot peening process using discrete-continuum coupling method. International Journal of Mechanical Sciences, 2016, (107): 21-33.

[20] C.B. Guo, S. Hu, D. Wang, Z. Wang Finite element analysis of the effect of the controlled parameters on plate forming induced by ultrasonic impact forming (UIF) process, Applied Surface Science, 2015, (353): 382-390.

[21] A. Gariepy, J. Cyr, A. Levers, C. Perron, P. Bocher, M. Levesque. Potential applications of peen forming finite element modelling. Advances in Engineering Software, 2012, (52): 60-71.

[22] J. Wu, P. Wei, H. Liu, B. Zhang, Guibao Tao, Effect of shot peening intensity on surface integrity of 18CrNiMo7-6 steel. Surface and coating technology, (2021) 127194.

[23] Q. Lin, H. Liu, C. Zhu, R. G. Parker, Investigation on the effect of shot peening coverage on the surface integrity. Applied Surface Science, 2019, (489): 66-72.

[24] J. Wu, H. Liu, P. Wei, Q. Lin, S. Zhou, Effect of shot peening coverage on residual stress and surface roughness of 18CrNiMo7-6 steel. International Journal of Mechanical Science, 2020, 105785.

[25] X. Cheng, Experimental and numerical approaches for improving rolling contact fatigue of bearing steel through enhanced compressive residual stress. Ohio. The Ohio State University,

2007.

[26] M. Kobayashi, T. Matsui, Y. Murakami, Mechanism of creation of compressive residual stress by shot peening. International Journal of Fatigue, 1998, 20(5):351-357.